

1 Validating Plutonium-239+240 as novel soil redistribution tracer - a
2 comparison to measured sediment yield

3 Katrin Meusburger^{1*}, Paolo Porto^{2,3}, Judith Kobler Waldis⁴, Christine Alewell⁴

4

5 ¹Swiss Federal Institute for Forest, Snow and Landscape Research WSL, CH-8903, Birmensdorf,
6 Switzerland.

7 ²Dipartimento di Agraria, Università degli Studi Mediterranea di Reggio Calabria, Reggio Calabria,
8 Italy.

9 ³Kazimierz Wielki University, Faculty of Geographical Sciences, Plac Kościeleckich 8, 85-033
10 Bydgoszcz, Poland.

11 ⁴Environmental Geosciences, University of Basel, Switzerland.

12

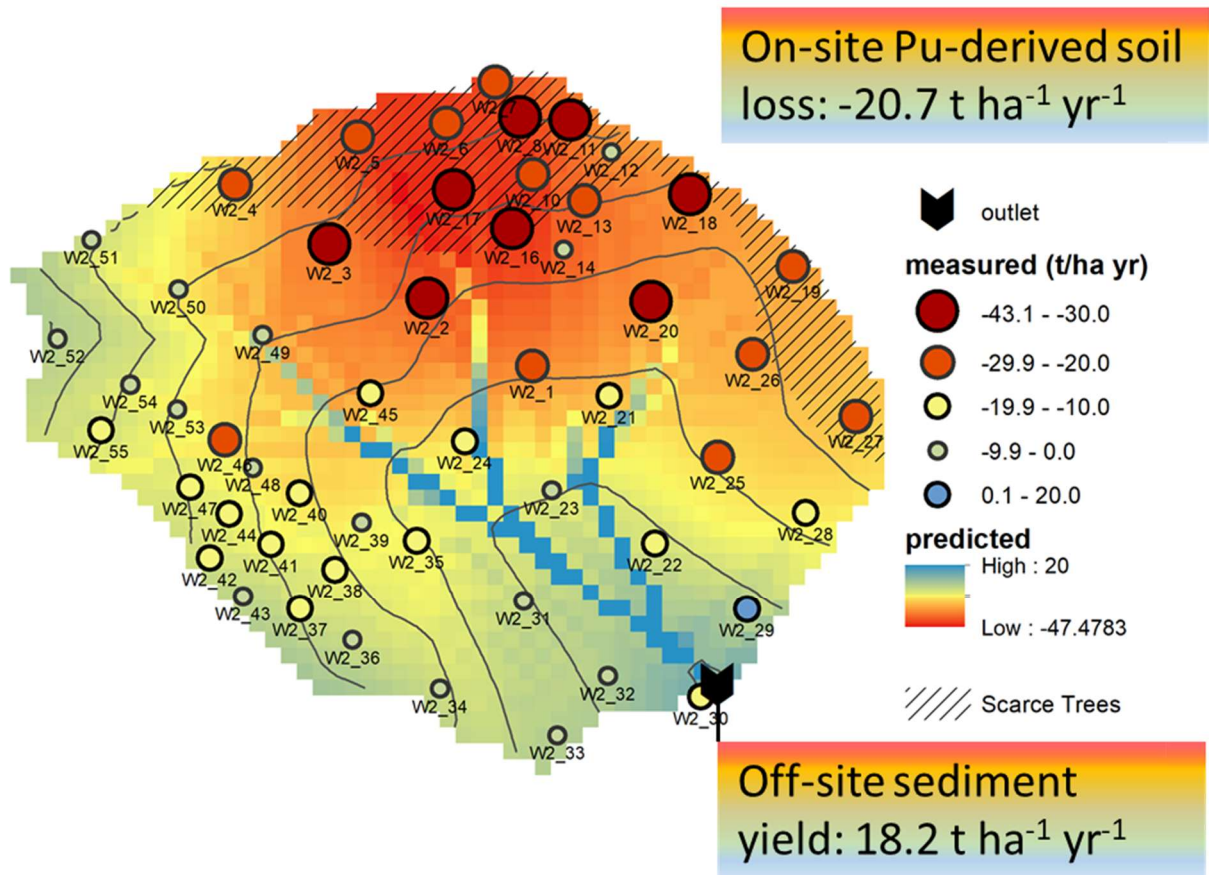
13 *corresponding author: Katrin.Meusburger@wsl.ch

14

15 **Abstract**

16 Quantifying soil redistribution rates is a global challenge addressed with direct sediment measurements
17 (e.g., traps), models and isotopic, geochemical and radionuclide tracers. The isotope of Plutonium,
18 namely $^{239+240}\text{Pu}$, is a relatively new soil redistribution tracer in this challenge. Direct validation of
19 $^{239+240}\text{Pu}$ as soil redistribution is, however, still missing. We used a unique sediment yield time series
20 in Southern Italy, reaching back to the initial fallout of $^{239+240}\text{Pu}$ to verify $^{239+240}\text{Pu}$ as a soil redistribution
21 tracer. Distributed soil samples (n=55) were collected in the catchment, and at undisturbed reference
22 sites (n=22), $^{239+240}\text{Pu}$ was extracted, measured with ICP-MS and converted to soil redistribution rates.
23 Finally, we used a Generalized Additive Model (GAM) to regionalize soil redistribution estimates for
24 the catchment. For the catchment sites, mean $^{239+240}\text{Pu}$ inventories were significantly reduced ($16.8 \pm$
25 10.2 Bq m^{-2}) compared to the reference inventory ($40.5 \pm 3.5 \text{ Bq m}^{-2}$) indicating the dominance of
26 erosion. Converting these inventory losses into soil erosion rates resulted in an average soil loss of 22.2
27 $\pm \text{SD } 7.2 \text{ t ha}^{-1} \text{ yr}^{-1}$. The uncertainties of the approach stemmed mainly from the high measurement
28 uncertainties of some low-activity samples where samples have been bulked over depth. Therefore, we
29 recommend taking incremental soil samples and extracting larger soil volumes (~20g). The geographic
30 coordinates and the flow accumulation best described the spatial pattern of erosion rates in the GAM
31 model. Using those predictors to upscale Pu-derived soil redistribution rates for the entire catchment
32 resulted in an average on-site loss of $20.7 \text{ t ha}^{-1} \text{ yr}^{-1}$, which corresponds very well to the long-term
33 average sediment yield of $18.7 \text{ t ha}^{-1} \text{ yr}^{-1}$ measured at the catchment outlet and to ^{137}Cs derived soil
34 redistribution rates. Overall, this comparison of Pu-derived soil redistribution rates with measured
35 sediment yield data validates $^{239+240}\text{Pu}$ as a suitable retrospective soil redistribution tracer.

36 **Graphical abstract**



37

38

39 1 Introduction

40 Soil erosion endangers climate and food security and has considerable adverse off-site effects on
41 freshwater systems (Reichstein et al., 2013; Amundson et al., 2015; Alewell et al., 2016; Panagos et al.,
42 2016; Borrelli et al., 2017; Alewell et al., 2020). Plutonium isotopes, with their previous hazardous
43 impacts on the environment and released as a product of thermonuclear weapons testing and from
44 nuclear accidents (e.g. Chernobyl), may serve as a tool to quantify long-term soil loss (Alewell et al.,
45 2017).

46 The approach to use $^{239+240}\text{Pu}$ as soil and sediment tracer is similar to other fallout radionuclides (FRN)
47 (Xu et al., 2015; Meusburger et al., 2018). Once deposited on the ground, FRNs strongly bind to soil
48 particles and move across the landscape primarily through physical soil redistribution processes (IAEA,
49 2014). In this way, fallout radionuclides provide an effective and retrospective (since the time of the
50 fallout) track of net soil and sediment redistribution (Zapata, 2003). However, ^{137}Cs , the most
51 commonly applied soil redistribution tracer, will reach its detection limit soon due to the successive
52 decay (half-life = 30.17 years). Thus, alternative tracers like excess Pb-210 and $^{239+240}\text{Pu}$ have been
53 explored (Wallbrink and Murray, 1996; Matisoff et al., 2002; Mabit et al., 2008; Kato et al., 2010; Porto
54 et al., 2013; Teramage et al., 2015; Xu et al., 2015; Meusburger et al., 2018). While Pb-210 is associated
55 with high uncertainties (Porto and Walling, 2012; Mabit et al., 2014; Meusburger et al., 2018), the
56 characteristics of $^{239+240}\text{Pu}$ seem more promising for soil tracing (Alewell et al., 2017).

57 The advent of $^{239+240}\text{Pu}$ as a soil redistribution tracer was accelerated by the adoption of the less time-
58 consuming (minutes instead of hours per sample) Inductively Coupled Plasma Mass spectrometry (ICP-
59 MS). It was a door opener for using $^{239+240}\text{Pu}$ as a soil erosion tracer. The application of $^{239+240}\text{Pu}$ comes
60 along with other advantages, such as i) reduced initial spatial variability at undisturbed, so-called
61 reference sites (Alewell et al., 2014; Meusburger et al., 2016), ii) less preferential uptake by plants
62 (Froehlich et al., 2016), iii) the possibility to assess the origin of the fallout by determining ^{240}Pu to
63 ^{239}Pu atom ratios or ^{137}Cs to $^{239+240}\text{Pu}$ activity ratios (Ketterer et al., 2004; Xu et al., 2013; Meusburger
64 et al., 2016; Meusburger et al., 2020), iv) considerably smaller soil sample volume needed for analysis,
65 and v) no decline due to decay, which is of particular relevance for locations with low initial ^{137}Cs
66 fallout such as the southern hemisphere (Tims et al., 2010). The potential of $^{239+240}\text{Pu}$ further convenes
67 with the availability of the new conversion model "Modelling Deposition and Erosion rates with
68 RadioNuclides (MODERN)", suitable for estimating soil redistribution rates by comparing reference
69 with soil redistribution affected inventories with any FRN (Arata et al., 2016a; Arata et al., 2016b).

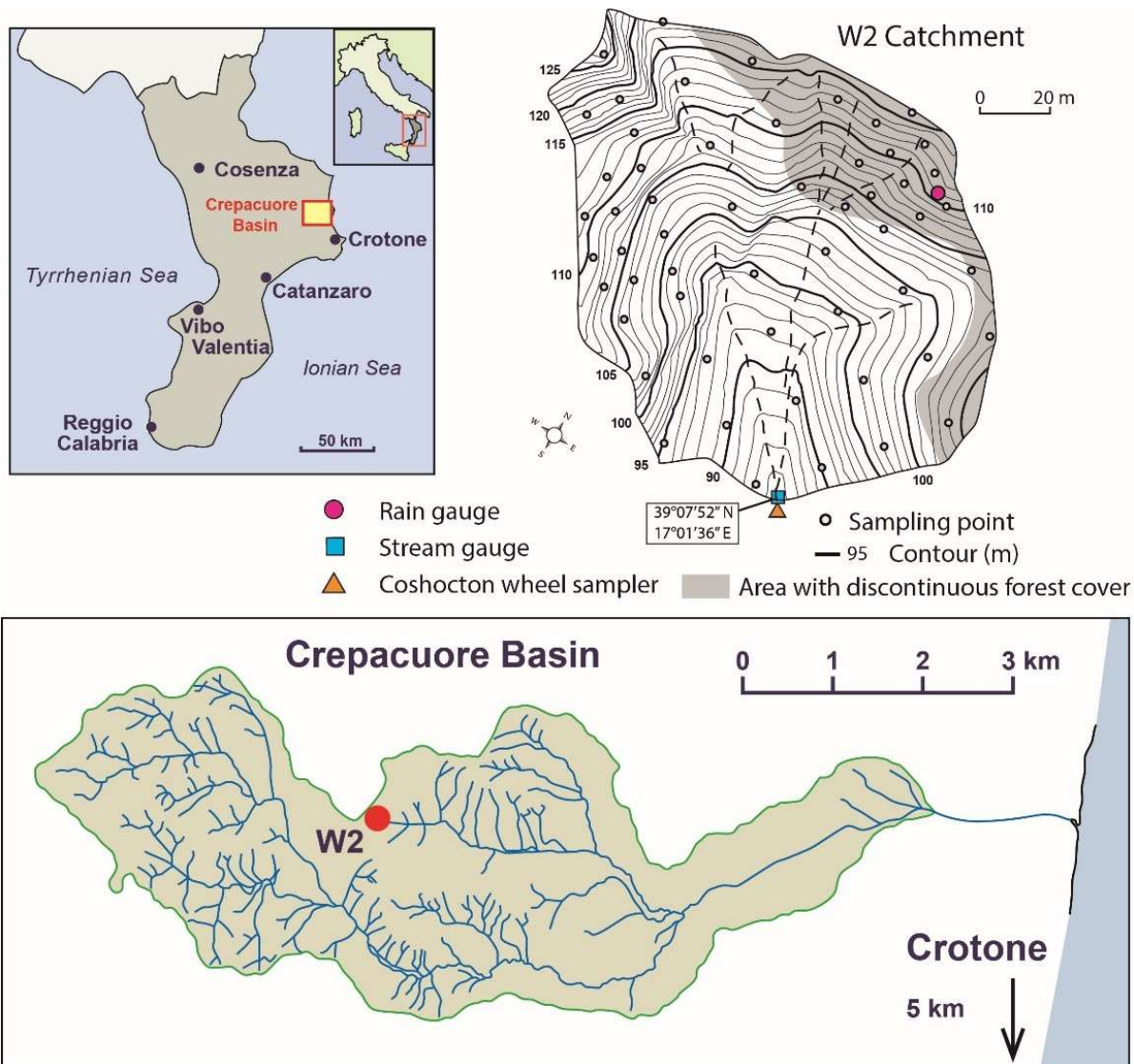
70 Several studies (Schimmack et al., 2001; Tims et al., 2010; Hoo et al., 2011; Lal et al., 2013; Michelotti
71 et al., 2013; Xu et al., 2013; Xu et al., 2015; Meusburger et al., 2018) have highlighted $^{239+240}\text{Pu}$'s
72 suitability as a soil redistribution tracer. However, to date, direct validation efforts to compare on-site
73 FRN-based soil erosion rates with off-site sediment yields have focused on other FRNs such as ^{137}Cs
74 and excess ^{210}Pb (Porto et al., 2001; Porto et al., 2003; Porto and Walling, 2012; Porto and Callegari,

75 2022). For $^{239+240}\text{Pu}$ -derived soil redistribution rates, such a direct validation is not achieved yet, to the
76 best of our knowledge. This study aims to fill this gap by validating $^{239+240}\text{Pu}$ -derived soil redistribution
77 rates with a long-term time series of measured catchment suspended sediment yields.

78 **2 Materials and Methods**

79 **2.1 Study site and soil sampling**

80 This study takes advantage of a unique long-term sediment yield monitoring catchment (W2, 1.38 ha)
81 located near Crotona in Calabria, Southern Italy (35 m a.s.l., 39°09'02"N, 17°08'10"E). The steep
82 catchment with a mean average slope of ca. 19° is located in the ephemeral headwaters of the larger
83 Crepacuore basin (Fig. 1). The geology of this area consists of Upper Pliocene and Quaternary materials
84 and produced soils with a clay loam texture with 14.6%, 49.2%, and 36.2% of sand, silt, and clay,
85 respectively. The catchment was never ploughed, but in 1968, *Eucalyptus occidentalis* Engl. was
86 planted and cut again in 1978 and 1990. The tree cover is partly patchy, with about 20% of the area on
87 south-facing slopes having discontinuous tree and grass cover. The climate is Mediterranean, with a
88 mean annual precipitation of ~670 mm, predominantly occurring from October to March.



89

90 Fig. 1 Location of the studied headwater catchment W2 within the Crepacuore Basin (lower panel
 91 indicated by a red dot), Calabria, Italy.

92 In 2014, the collection of soil samples in the catchment was undertaken along an approximate 20 m ×
 93 20 m grid with additional cores collected from areas characterized by marked variability of vegetation
 94 cover and topography with slopes from 5° to 35° (Fig. 1). The samples were taken with a steel core tube
 95 (10 cm diameter) driven into the ground to a depth of 15 cm by a motorized percussion corer and
 96 subsequently extracted using a hand-operated winch. For each sampling point, two cores were taken,
 97 and they were bulked before analysis. This procedure provided a total of 55 composite bulk cores over
 98 the catchment area.

99 In March 2021, a new sampling campaign was undertaken to obtain information at the reference area
 100 to establish the baseline for $^{239+240}\text{Pu}$ in the area. In this case, 3 depth profiles and 19 additional bulk
 101 reference soil cores were collected in adjacent undisturbed rangeland with some scattered oaks
 102 (*Quercus pubescens*) at a similar altitude to the study catchment (see Porto and Callegari, 2022). The

103 area has very low slope gradients ($<2^\circ$) and it is located on top of a hill. As such, the sampling point did
104 not receive run-on surface flow from positions immediately upslope. Further, we avoided sampling the
105 areas covered by canopy to minimize the interzeption effects. Each sampling point was carefully chosen
106 in the clearing areas far from the tree trunks to avoid also problems due to stemflow.

107 The samples were collected using the same sampling device consisting of a motorized soil column
108 cylinder auger set in which a core tube (60 cm in length) with a larger internal diameter (11 cm) is
109 accommodated. The three depth profiles were sectioned into increments of 2 cm and were analyzed
110 separately for ^{137}Cs and $^{239+240}\text{Pu}$ content. Before radiometric analyses, all samples were dried and sieved
111 to <2 mm. In a previous study, the soil samples collected within the catchment were analyzed for ^{137}Cs
112 using high-resolution HPGe detectors available at the Agraria Department at the University
113 Mediterranea of Reggio Calabria, Italy (Porto et al., 2014). Counting times for the samples collected
114 during that campaign were ca. 80,000 s, providing a precision of ca. $\pm 10\%$ at the 95% confidence level.
115 The reference samples of 2021 were also analyzed for ^{137}Cs with the same detector settings. All ^{137}Cs
116 measurements were decay corrected to 01.01.2014 and used to calculate $^{239+240}\text{Pu}$ to ^{137}Cs activity ratios.

117 **2.2 Extraction of $^{239+240}\text{Pu}$ and mass spectrometry for atom ratio and concentration** 118 **measurements**

119 All samples (5-10g) were oven-dried at 105°C for 48 h, mechanically disaggregated and dry-sieved to
120 recover the <2 mm fraction. First, a representative sub-sample of this fraction was spiked with ~ 0.005
121 Bq of a ^{242}Pu yield tracer (licensed solution from NIST). Next, Pu was leached with 16M nitric acid
122 overnight at 80°C and separated from the leach solution using a Pu-selective TEVA resin (Ketterer et
123 al., 2011). The isotope dilution calculations determined the masses of ^{239}Pu and ^{240}Pu present in the
124 sample and converted them into the summed $^{239+240}\text{Pu}$ activity. The analysis was done with a Thermo
125 X7 quadrupole ICP-MS system at Universidad de Cádiz. Please refer to Meusburger et al. (2020) for
126 details on the instrument method.

127 The information of $^{239+240}\text{Pu}$ in relation to ^{137}Cs allows for assessing the origin of the fallout (e.g.,
128 Chernobyl derived versus global bomb fallout). A prerequisite for using the ^{137}Cs to $^{239+240}\text{Pu}$ activity
129 ratio is that Pu is exclusively derived from global fallout. Thus, in a first step, the ^{240}Pu to ^{239}Pu atom
130 ratios around 0.18 confirmed the $^{239+240}\text{Pu}$ origin merely from global bomb fallout (Kelley et al., 1999).
131 In a second step, ^{137}Cs to $^{239+240}\text{Pu}$ activity ratios reveal the percentage of bomb derived (ratio 0.027)
132 versus Chernobyl derived (ratio 0.013) (Ketterer et al., 2004; Xu et al., 2013; Meusburger et al., 2016;
133 Meusburger et al., 2020).

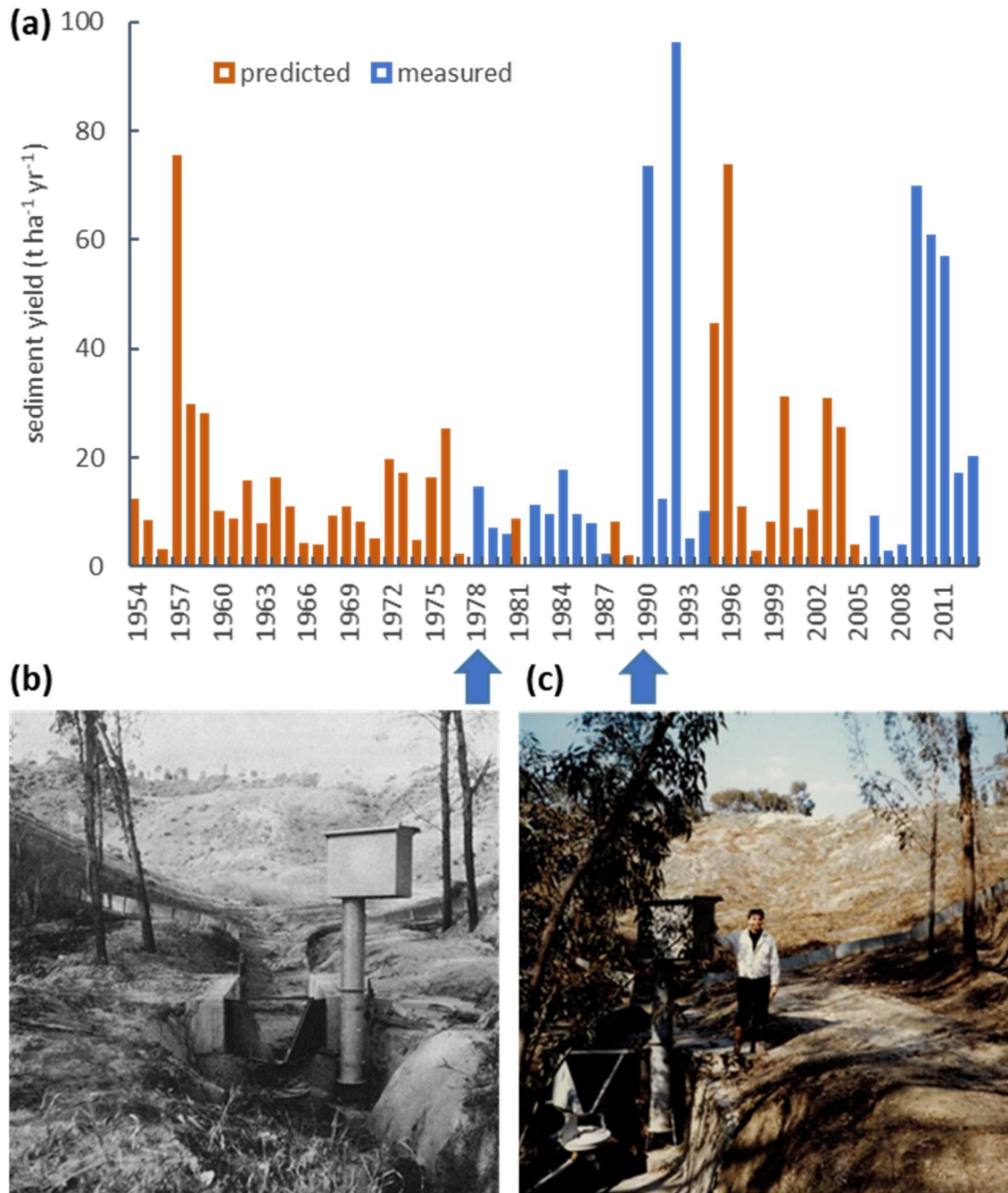
134 **2.3 Conversion of Pu-239+240 activities to soil redistribution rates**

135 The total inventory (Bq m^{-2}) of each bulk soil core was calculated as the product of the measured
136 $^{239+240}\text{Pu}$ activity (Bq kg^{-1}) and the dry mass of the <2 mm fraction of the bulk core (kg), divided by the
137 surface area associated with the soil core (m^2). The inventories were converted into soil redistribution
138 rates using the Profile Distribution model PDM (Walling et al., 2002; Walling et al., 2014) and the
139 model Modelling Deposition and Erosion rates with RadioNuclides (MODERN (Arata et al., 2016a;
140 Arata et al., 2016b)). The profile distribution model is commonly employed to interpret the shape of an
141 FRN along the soil profile. It assumes an exponential depth distribution, and the depth of soil removed
142 by erosion is estimated by comparing the reduction in the FRN inventory with that related to the
143 reference site (see Porto et al., 2003). MODERN aligns the sampling site's total inventory to the
144 measured shape of the reference site's depth profile to estimate the thickness of soil losses/gains. The
145 intersection along the soil profile represents the solution of the model. We selected 1963 as the reference
146 year for the erosion rate conversion. In 1963, the main global fallout peak occurred, commonly used in
147 conversion models (Walling et al., 2002). The PDM equation was implemented in R, while MODERN
148 was calculated with Matlab R2022b.

149 We accounted for the uncertainty in the conversion procedure by running both conversion models 100
150 times, sampling from the reference and the erosion inventory within the uncertainty bounds and for the
151 PDM in addition to the shape factor h_0 . The sampling was done from normal distributions, defined by
152 the mean measured value and the standard deviations (SD): i) of the repeated ICP-MS measurements
153 for the erosional sites, ii) of the replicate reference inventories, iii) of the three depth profiles for the h_0
154 factor (**Error! Reference source not found.**).

155 2.4 Sediment yield measurements

156 Since 1978, precipitation, runoff and sediment yield have been measured in the W2 catchment (Cantore
157 et al., 1994). Precipitation was recorded using a tipping bucket rain gauge, and runoff was measured at
158 the outlet using an H-flume structure equipped with a mechanical stage recorder. Below the H-flume,
159 the sediment load was measured with a Coshocton wheel sampler (Porto et al., 2003). Sediment yield
160 data used in this analysis is related to the period from 1978 to 1994 (Cantore et al., 1994) and from 2006
161 to 2013 (Fig. 2). However, due to the malfunctioning of the sediment sampling equipment in the
162 catchment during some events, direct measurements of total annual sediment yield values are not
163 available for all years. To account for these missing years, the corresponding sediment output was
164 estimated using the Arnoldus Index, for which long-term observations are available from the station of
165 Crotone located ca. 10 km distant from the study catchment (see Capra et al., 2017). The standard error
166 of this regression was $23 \text{ t ha}^{-1} \text{ yr}^{-1}$. These estimates were then incorporated into the annual record of
167 sediment yield (Fig. 2), and the sediment yield data was extrapolated to cover the period 1963–2013,
168 corresponding to the period captured by $^{239+240}\text{Pu}$ derived soil redistribution assessments.



169

170 Fig. 2 Measured (orange) and predicted (blue) annual sediment yield (t ha⁻¹ yr⁻¹) of the headwater
 171 catchment W2 (a). Predictions of sediment yields are based on a significant relation to Arnoldus
 172 erosivity index. In 1968, *Eucalyptus occidentalis* Engl. was planted in the catchment that was harvested
 173 in 1978 (b) (photo by M. Raglione, from Avolio et al., (1980)) and a second time in 1990 (c).

174 **2.5 Spatial extrapolation of ²³⁹⁺²⁴⁰Pu derived estimates**

175 We used a generalized additive model (GAM) to upscale the point erosion estimates to the entire
 176 catchment. Spatially explicit soil redistribution rates for the entire catchment are needed to enable the
 177 comparison to the sediment yields measured at the catchment's outlet. Therefore, GAMs were fitted to
 178 the measured erosion estimates using spatially explicit covariates. As spatial covariates, elevation,

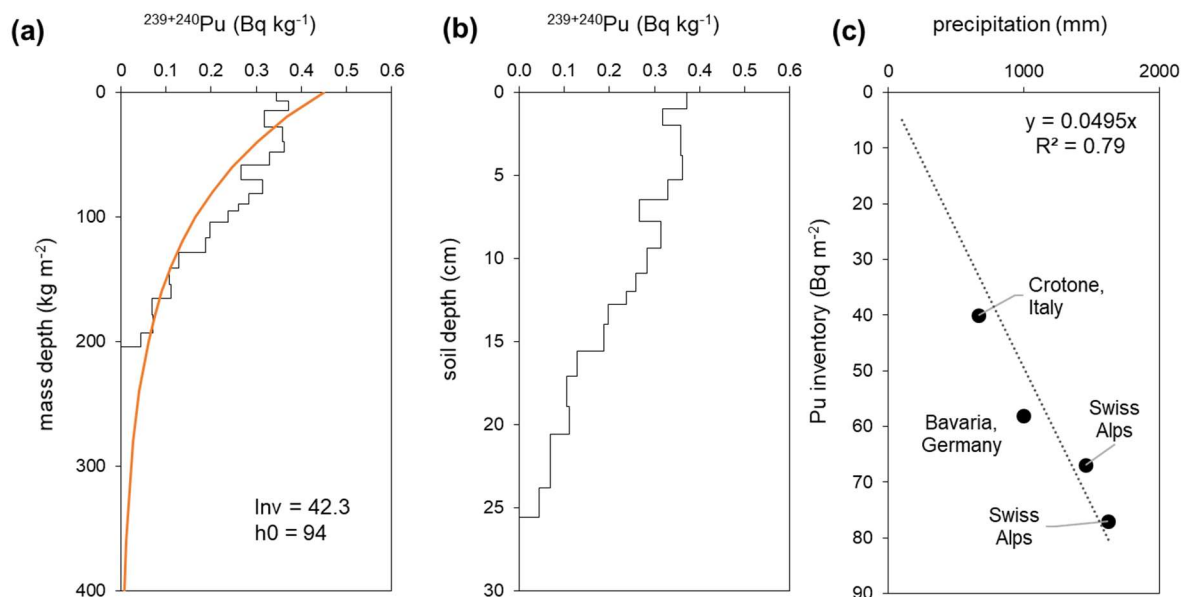
179 slope, aspect, flow accumulation, and scarce, discontinuous tree cover (as 0 and 1 categorical variables,
180 see Fig. 1) were tested. These covariates were derived from a DEM with 3m spatial resolution using the
181 terrain function from the raster package. Because of the small sample size of 55 sites, only a maximum
182 of three covariables could be added to the model. For cross-validation (n=50) of the spatial prediction,
183 the data were randomly split into 80% training and 20% testing data. GAMs can account for nonlinear
184 relationships by coefficients that can be expanded as smooth functions of covariates. These smooth
185 terms were modelled by splines, and geographic coordinates (x and y) were modelled as a 2d spline. To
186 prevent overfitting, we used the restricted maximum likelihood (REML) method with the R package
187 mgcv (Wood, 2006).

188 **3 Results and Discussion**

189 **3.1 ²³⁹⁺²⁴⁰Pu distribution at the reference sites**

190 The mean measured ²⁴⁰Pu to ²³⁹Pu atom ratios at the reference and sampling sites were 0.18±0.03
191 (Kelley et al., 1999). These atom ratios corresponded to the atom ratio found for the global fallout
192 (Kelley et al., 1999) and confirmed global fallout as the sole source of Pu in the catchment.

193 The three reference depth profiles ²³⁹⁺²⁴⁰Pu activity at the reference site showed different shapes with
194 soil depth (**Error! Reference source not found.**). While profile 2 displays the expected exponential
195 decline with soil depth, profile 1 shows signs typically expected from erosional processes and profile 3
196 of depositional processes (**Error! Reference source not found.**).
197 Therefore, only profile 2 was assessed to be suitable for extracting the shape of the depth distribution
198 for the conversion procedure (Fig. 3a). The penetration depth of ²³⁹⁺²⁴⁰Pu reached 205 kg m⁻²,
199 corresponding to 26 cm soil depth (Fig. 3b). With an exponential model fit of the PDM, we derived an
200 h₀ at 94 kg m⁻², representing the point where half of the activity is stored. The mean ²³⁹⁺²⁴⁰Pu reference
201 inventory was estimated at 42.3±3.5 Bq m⁻². The surface soil (0 cm) concentration, which was derived
202 by fitting an exponential model, was 0.45 Bq kg⁻¹ (Fig. 3a).



203

204 Fig. 3 (a) $^{239+240}\text{Pu}$ activity with soil mass depth measured at the reference site (selected profile 2). Inv
 205 corresponds to the total inventory of the soil, and h_0 to the shape factor of the exponential fit (orange).
 206 (b) $^{239+240}\text{Pu}$ activity with soil depth (cm) at the reference site (profile 2). (c) Relation between Pu
 207 reference inventories and precipitation for European studies (Schimmack et al., 2001; Alewell et al.,
 208 2014; Meusburger et al., 2018).

209 The $^{239+240}\text{Pu}$ measurements of the 19 bulk reference soil cores showed a bimodal distribution with six
 210 high inventories clustering at a mean of $40.2 \pm 4.4 \text{ Bq m}^{-2}$ and 13 low inventories of $15.0 \pm 2.8 \text{ Bq m}^{-2}$.
 211 The $^{239+240}\text{Pu}$ activities of the bulk soil cores with low inventories had activity values $< 0.043 \text{ Bq kg}^{-1}$,
 212 close to the detection limit, and the standard deviation of replicate measurement of these samples was
 213 high. We calculated the Pu to Cs activity ratios to verify the plausibility of these low inventories. For
 214 European soil samples, the activity ratio of Pu to Cs (with Cs being decay corrected to 2014) is expected
 215 between 81 and 24 (Meusburger et al., 2020). However, the low inventory bulk cores had mean Pu/Cs
 216 ratios of 156, which is clearly outside this range. A possible explanation for these very low Pu values
 217 in the reference site might be the mixing and dilution of deeper layers with no Pu activity into the bulk
 218 reference soil cores. Therefore, these low-reference bulk samples were removed from further analysis.
 219 Bulking of Pu samples causing a dilution of the Pu activity should be avoided, particularly in areas of
 220 high erosion or low initial fallout (Wilken et al., 2021). Here, we resolved the dilution problem due to
 221 the availability of ^{137}Cs data, as the ^{137}Cs to $^{239+240}\text{Pu}$ activity ratios were valuable in identifying the
 222 suitability of the reference samples. The plausibility of the Pu inventory was further underpinned when
 223 the inventory was related to the mean annual precipitation of other published European studies (Fig.
 224 3c). The few published Pu inventories in Europe (Schimmack et al., 2001; Alewell et al., 2014;
 225 Meusburger et al., 2018) show a linear relation to mean annual precipitation with 77, 67, 58 Bq m^{-2} for
 226 1650, 1450, 950 mm of rainfall. The high inventory of this study of 40.2 Bq m^{-2} plots on the linear
 227 relation (Fig. 3c), while the low inventory of 15 Bq m^{-2} is below the expected amount given the

228 catchment's mean annual precipitation. Taking the depth distribution reference and only the six high
229 inventories of bulk soil cores into account, the mean reference inventory of the soil profiles was 40.5
230 \pm 3.5 Bq m⁻² with a coefficient of variation of 8.6%. In the context of other Pu studies conducted in
231 Europe, our inventories are at the lower end of the spectrum due to the low rainfall in these
232 Mediterranean regions. However, in the context of global studies, even lower Pu inventories are
233 common, e.g. in the Kongo with 8.0-24.4 Bq m⁻² in non-forested reference sites (Wilken et al., 2021)
234 and Australia with 8.8 Bq m⁻² (Lal et al., 2013).

235 All in all, following the above-described procedure, the ²³⁹⁺²⁴⁰Pu reference inventories had a small
236 spatial variability with a CV of <9%. For ¹³⁷Cs, the CV was 11.6% in the same reference area (see Porto
237 and Callegari, 2022). The spatial variability of Pu in reference sites was comparable to previous studies
238 (Alewell et al., 2014; Meusburger et al., 2016).

239 **3.2 Catchment inventories and soil redistribution rates at sampling points**

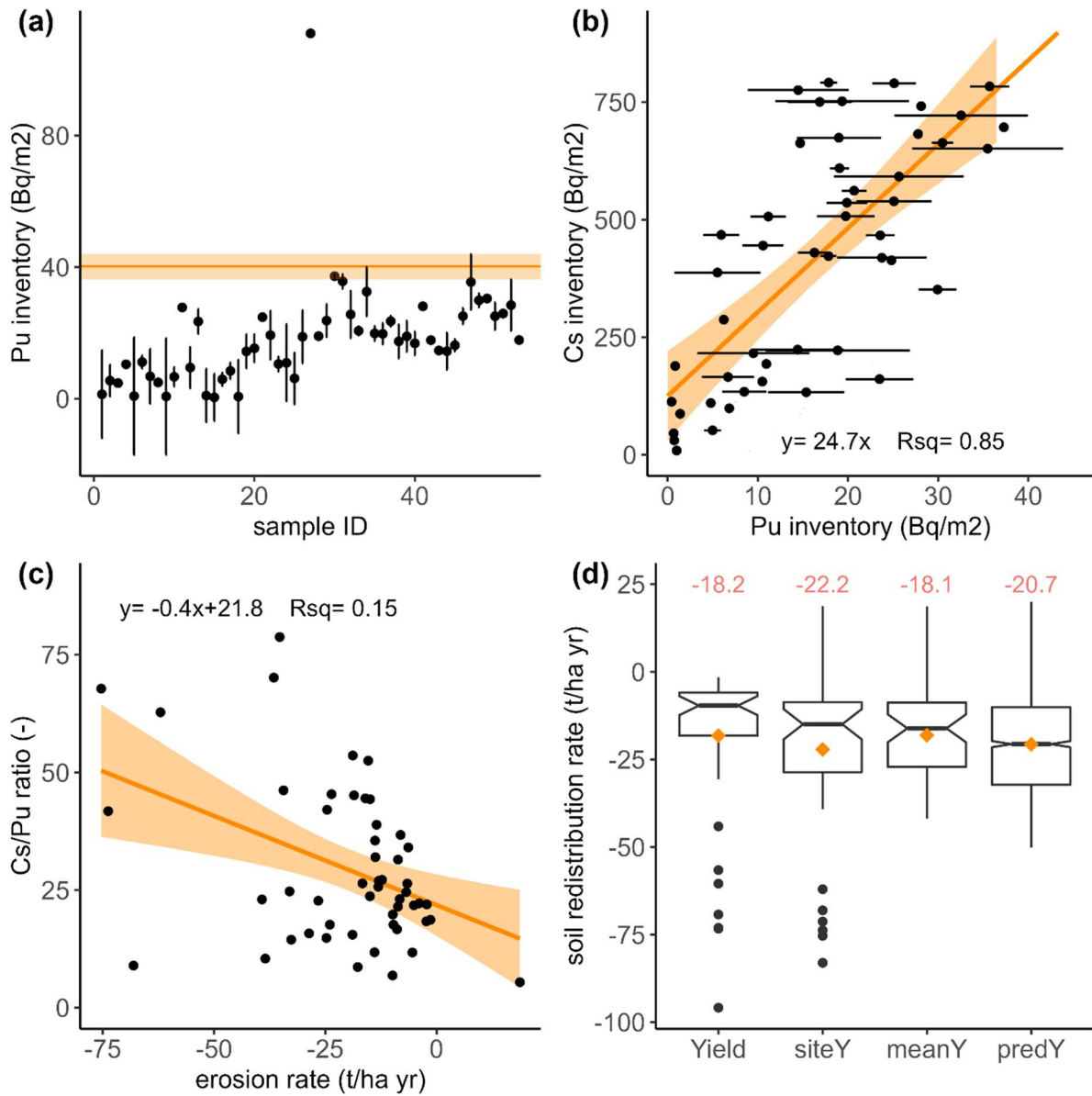
240 The ²³⁹⁺²⁴⁰Pu activities at the sampling sites ranged from 0.001 to 0.143 Bq kg⁻¹ with a mean of 0.066
241 Bq kg⁻¹. The uncertainties of repeated ICP-MS measurements increase with decreasing activities from
242 the smallest SD of 0.0004 Bq kg⁻¹ to the largest of 0.067 Bq kg⁻¹, corresponding to <1% to larger >24%
243 of the measured activity with a mean of 2% (Supplementary Figure 3).

244 The respective mean ²³⁹⁺²⁴⁰Pu inventories for all 55 sites were 16.8 Bq m⁻² with a spatial SD of \pm 10.2
245 Bq m⁻², thus less than half of the reference inventory. Given the uncertainty bounds, all inventories,
246 except for four sites, were significantly smaller than the reference inventory, indicating soil erosion
247 (Fig. 4a). One site close to the catchment outlet had a very high ²³⁹⁺²⁴⁰Pu inventory of 111 Bq m⁻²
248 exceeding the reference inventory by almost three times (Fig. 4a). The ²³⁹⁺²⁴⁰Pu inventories are
249 significantly ($p < 0.001$) correlated to the ¹³⁷Cs inventories with 24.7 times more Bq m⁻² for ¹³⁷Cs (Fig.
250 4b). The Cs/Pu activity ratios of the catchment sites were at the lower range of the plausible fallout
251 range (between 23.9 = global and 81.3 = Chernobyl) with a mean value of 24.7. The activity ratios are
252 significantly ($p < 0.005$) decreasing with decreasing erosion rates even though R² of the regression is
253 with 0.15 very low (Fig. 4c).

254 This depletion in ¹³⁷Cs pointed towards a preferential loss of ¹³⁷Cs during soil loss. A possible
255 explanation might be that ¹³⁷Cs is transported with different soil particles as Pu, which are more
256 susceptible to soil erosion. It is known that ²³⁹⁺²⁴⁰Pu exhibits a different sorption behaviour to soil
257 particles compared to, e.g. ¹³⁷Cs. Pu is mainly associated with organic matter and sesquioxides in
258 addition to clay particles, whereas ¹³⁷Cs is predominantly bound to the fine mineral clay fraction
259 (Lujanienė et al., 2002; Qiao et al., 2012; Meusburger et al., 2016; Xu et al., 2017). As a consequence,
260 ²³⁹⁺²⁴⁰Pu is more exchangeable and might more easily migrate downward in soils (Schimmack et al.,
261 2001; Meusburger et al., 2016). This different sorption behaviour may result in different depth

262 distributions, which have important implications for its use as a soil erosion tracer, e.g. regarding the
 263 conversion of measured FRN inventory changes into soil redistribution rates. Further, it may also have
 264 implications regarding interpreting ^{137}Cs to $^{239+240}\text{Pu}$ activity ratios that may be shifted outside the
 265 expected ranges at sites affected by soil redistribution.

266



267

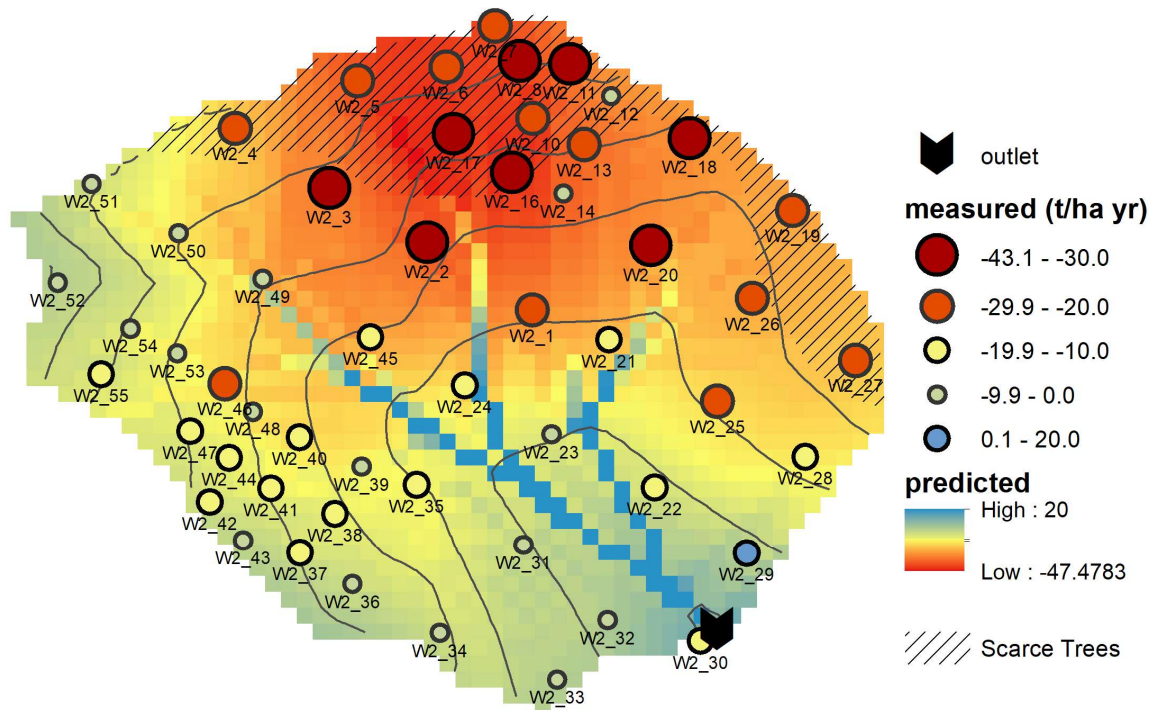
268 Fig. 4 (a) $^{239+240}\text{Pu}$ inventories with measurement errors in relation to sample ID (points) and the
 269 reference inventory (orange line with ribbon). (b) Relation between $^{239+240}\text{Pu}$ and ^{137}Cs inventories (error
 270 bars indicate the measurement error for Pu) with a linear trend line. (c) Activity ratio of Cs to Pu versus
 271 erosion rate. (d) Measured sediment yield at catchment outlet (Yield), Pu-derived erosion rates based
 272 on measured inventories within the catchment (siteY) and as a mean of the repeated conversion results
 273 (meanY), and mean of regionalized catchment Pu-derived erosion rates (predY). Orange points and text
 274 show the mean values of each approach.

275 3.3 Comparison of ²³⁹⁺²⁴⁰Pu derived soil redistribution rates and sediment yield of the 276 catchment

277 Soil redistribution rates obtained from the established conversion model PDM and the relatively new
278 MODERN agree very well (**Error! Reference source not found.**). This agrees with previous
279 comparisons done for different conversion models and FRNs (Meusburger et al., 2018). We produced
280 three sets of Pu-derived soil redistribution rates using i) direct conversion of the site inventories (siteY)
281 and ii) the average of 100 Monte Carlo conversion models per site generated by sampling within the
282 uncertainty ranges of all input parameters (meanY) and iii) regionalized estimates for the catchment
283 (predY). For the point estimates will refer to these meanY in the following because the uncertainty
284 related to the entire procedure is included in this second set of redistribution rates.

285 Soil redistribution rates were highly variable within the catchment (Fig. 5). The highest soil loss with
286 $43 \pm 20 \text{ t ha}^{-1} \text{ yr}^{-1}$ occurred in the upper part with patchy tree cover. Generally, the sites with scarce tree
287 cover and adjacent sites showed the highest soil erosion rates. Downslope and towards the outlet of the
288 catchment, the erosion rates decrease. Close to the outlet, soil deposition of $18.7 \pm 2.0 \text{ t ha}^{-1} \text{ yr}^{-1}$ was
289 observed in one measurement point (W2_29). The deposition rate is, however, difficult to quantify
290 without knowledge of the respective soil source area or a Pu depth profile in the deposition site. The
291 average of all measured site redistribution rates (siteY) indicated erosion of $-22.2 \text{ t ha}^{-1} \text{ yr}^{-1}$ with a spatial
292 standard deviation of $\pm 21.1 \text{ t ha}^{-1} \text{ yr}^{-1}$. On average, the standard deviation, derived from repeated Monte
293 Carlo conversions, of these redistribution rates were $7.2 \text{ t ha}^{-1} \text{ yr}^{-1}$, with a slightly lower median of the
294 standard deviations of $4.2 \text{ t ha}^{-1} \text{ yr}^{-1}$ corresponding to a mean CV of 45% and a median CV of 36%.
295 Generally, higher erosion estimates are subject to higher standard deviations resulting from higher
296 uncertainties for measuring low Pu activities. Excluding these measurement uncertainties from the
297 Monte Carlo conversion reduced the CV of the erosion estimates to mean and median CVs of 19% and
298 13%, respectively.

299 The XY-coordinates, elevation, and flow accumulation best explained the spatial pattern of soil
300 redistribution rates. The deviance explained with these two spatial covariates was 56.7%, with lower
301 accuracy of 24% for the cross-validation procedure. The spatial pattern of the predicted soil
302 redistribution rates showed erosion in most of the catchment (Fig. 5). Only in grid cells with high flow
303 accumulation deposition occurred. The average redistribution rate from the grid cells (predY) amounted
304 to $-20.7 \text{ t ha}^{-1} \text{ yr}^{-1}$ (Fig 4d). Given the mean measured sediment yield at the outlet (Yield) of -18.2 t
305 $\text{ha}^{-1} \text{ yr}^{-1}$ (standard deviation between years of $21.8 \text{ t ha}^{-1} \text{ yr}^{-1}$), this corresponds to a 14% overestimation
306 of the mean soil loss by the Pu method (Fig 4d). The sediment yield (Yield) corresponds to the off-site
307 net erosion over time while the Pu-derived rates (siteY, meanY and predY) to the on-site erosion over
308 space. Their correspondence indicates that most of the on-site eroded sediments are delivered to the
309 outlet of the stream channel within the considered period.



310

311 Fig. 5 Soil redistribution rates assessed with Pu-derived soil redistribution rates (points) and spatial
 312 prediction of soil redistribution rates based on these point rates using XY-coordinates, elevation and
 313 flow accumulation as spatial covariates.

314 The Pu-derived soil erosion rates in the catchment were very high, with maximum values $<-40 \text{ t ha}^{-1} \text{ yr}^{-1}$
 315 ¹. However, documented soil erosion peaks in this area can reach up to $100\text{--}150 \text{ t ha}^{-1} \text{ yr}^{-1}$ during
 316 exceptional rainfall events (Porto et al., 2018; Porto et al., 2022). The sediment yield time series reveals
 317 that besides the rainfall erosivity, particularly the second harvest of eucalyptus trees (1990), triggered
 318 soil erosion. The soil conservation effect of the eucalyptus trees was also revealed by the lower Pu
 319 inventory and, therefore, higher soil losses in the catchment area with scarce tree cover. The protective
 320 effect of trees (Sorriso-Valvo et al., 1995; Zhou et al., 2002) and vegetation cover, in general, was also
 321 found in other studies and reviewed by Zuazo and Pleguezuelo (2009). Flow accumulation, a proxy for
 322 runoff concentration in a catchment, was an important predictor of soil erosion patterns. Interestingly,
 323 the relationship was negative with lower soil losses and higher chances for deposition with increasing
 324 flow accumulation. A reason for this was likely the collinearity between decreasing slopes with
 325 increasing flow accumulation, reducing the sediment transport capacity (Xiao et al., 2017). Still, flow
 326 accumulation performed better than alternative GAM models, including slope.

327 Mean ²³⁹⁺²⁴⁰Pu-based mean soil redistribution rates were $-20.7 \text{ t ha}^{-1} \text{ yr}^{-1}$ and 14% higher as measured
 328 sediment yields at the catchment outlet. Given both methods' uncertainties and variability, comparable
 329 magnitudes were achieved. In a recent study, Porto and Callegari (2022) found ¹³⁷Cs redistribution mean
 330 rates of $-20.4 \text{ t ha}^{-1} \text{ yr}^{-1}$. The ¹³⁷Cs and ²³⁹⁺²⁴⁰Pu derived soil redistribution rates are in good agreement.

331 **4 Conclusion**

332 Recent measurements of $^{239+240}\text{Pu}$ in a catchment in Southern Italy provided essential insights into the
333 suitability of the $^{239+240}\text{Pu}$ technique to estimate soil erosion rates. We also rigorously tested the
334 uncertainties involved in the approach. In our case study, the highest uncertainty resulted from the high
335 measurement uncertainty of low inventory samples, with a median CV of 21% and a high measurement
336 uncertainty of <1% – 100%. This high uncertainty can, for future studies, be minimized by (i) taking
337 incremental soil depth samples, avoiding dilution with deeper horizons of low-activity soil, and (ii)
338 extracting Pu on larger soil samples to reach Pu activities $>0.02 \text{ Bq kg}^{-1}$. Based on values with adequate
339 measurement certainty, the $^{239+240}\text{Pu}$ technique showed a low spatial variability of the reference
340 inventory (CV <9%) and the shape of the Pu distribution within the soil profile proved stable adsorption
341 to the topsoil. Patterns of inventory loss were related to soil redistribution processes, with the best spatial
342 predictors being tree cover and flow accumulation. The Pu-assessed redistribution rates were in
343 agreement with ^{137}Cs -derived rates and sediment yield measurements at the catchment outlet.

344 Increasing climatic extremes associated with more intense farming practices endanger our soil
345 resources, and new tools to monitor soil losses are of utmost importance. So far, the tracer ^{137}Cs has
346 been a powerful approach to assess soil redistribution rates since its fallout. However, alternative tracers
347 are needed in light of the subsequent decay of ^{137}Cs approaching the detection limit. In most aspects,
348 the $^{239+240}\text{Pu}$ technique works analogue to the ^{137}Cs technique. However, sample preparation with
349 extraction is more demanding and destructive to the soil, while for the ^{137}Cs method soils are only sieved
350 and dried and might be re-used for further analysis. We conclude that $^{239+240}\text{Pu}$, with its considerably
351 longer half-life, is a suitable and promising soil redistribution tracer.

352

353 **Data availability**

354 The authors declare that all other data supporting the findings of this study are available within the
355 article and its Supplementary Information files.

356 **Acknowledgements**

357 We thank the University of Cadiz for measuring $^{239+240}\text{Pu}$ on the ICP-MS.

358 **Author information**

359 **Contributions**

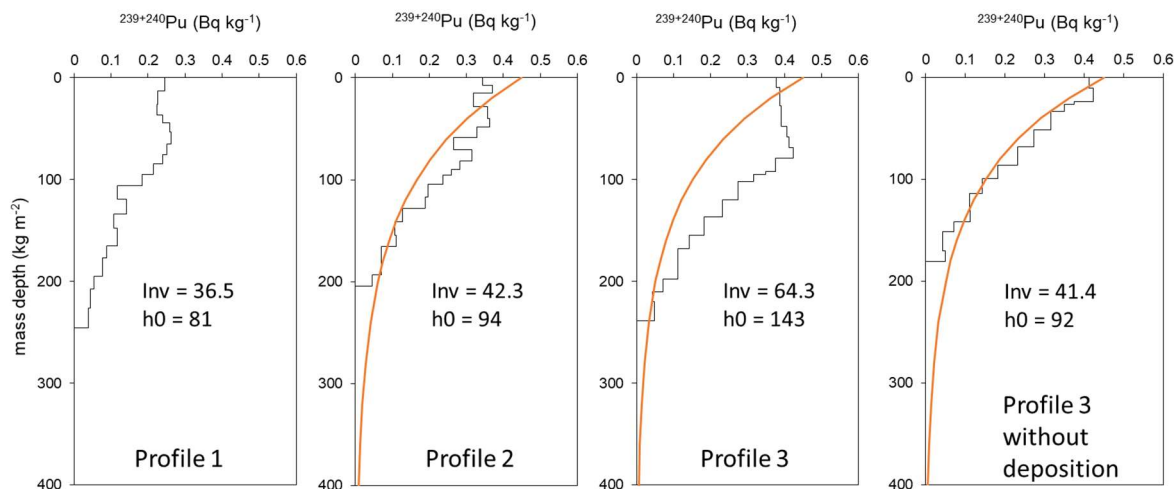
360 K.M., C.A, and P. P. conceptualized the study. P.P. collected the samples, J.K.-W. measured them and
361 calculated the measurement uncertainties. K.M. and P.P. did the data analysis. K.M. wrote the
362 manuscript, and all co-authors contributed to the writing process.

363 **Competing interests**

364 The authors declare no competing financial interests.

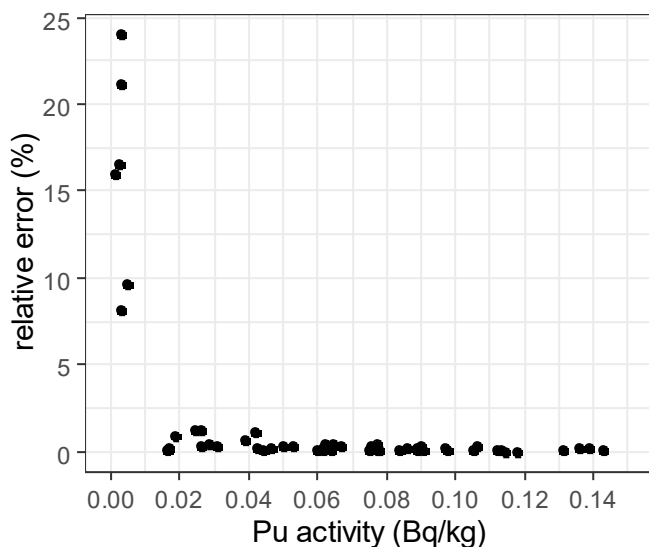
365

366 **Supplementary Information**



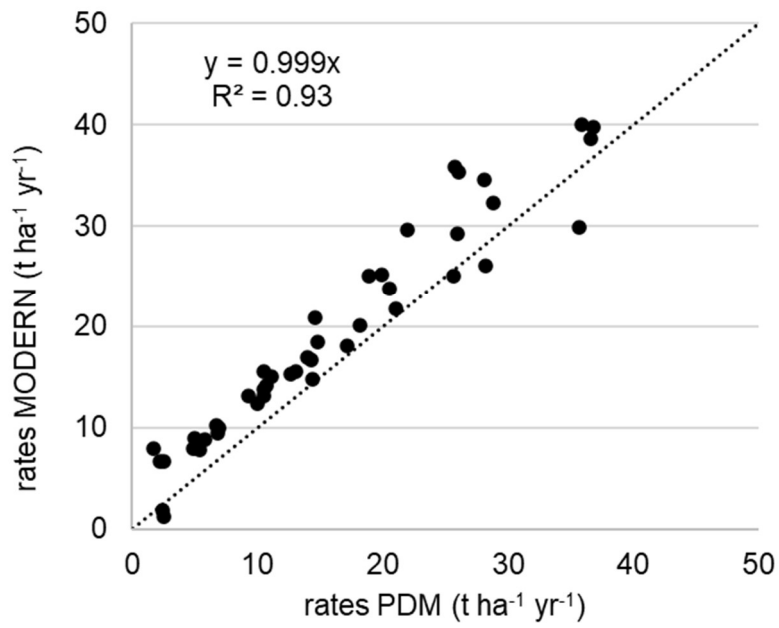
367

368 Supplementary Figure 1 Pu-239+240 activity with soil mass depth measured at three potential reference
 369 sites. Inv corresponds to the total inventory of the soil, and h₀ to the shape factor of the exponential fit
 370 (orange). Profile 3 was fitted with and without deposition layers. The standard deviation of the depth
 371 distribution and h₀ factor of profiles 1, 2 and 3 (without deposition) was used for the uncertainty
 372 assessment in the conversion model.



373

374 Supplementary Figure 2 Relative error (%) of replicate $^{239+240}\text{Pu}$ activity measurements with a
 375 quadrupole ICP-MS. At low activities the relative error of the measurements increased.



376

377 Supplementary Figure 3 Comparison of soil erosion rates between the Profile distribution conversion
 378 model (PDM) and the Modelling Deposition and Erosion rates with RadioNuclides (MODERN).

379 **References**

- 380 Alewell, C., Meusburger, K., Juretzko, G., Mabit, L., and Ketterer, M. E.: Suitability of $^{239+240}\text{Pu}$ and
381 ^{137}Cs as tracers for soil erosion assessment in mountain grasslands, *Chemosphere*, 103, 274–280,
382 10.1016/j.chemosphere.2013.12.016, 2014.
- 383 Alewell, C., Birkholz, A., Meusburger, K., Schindler Wildhaber, Y., and Mabit, L.: Quantitative
384 sediment source attribution with compound-specific isotope analysis in a C3 plant-dominated
385 catchment (central Switzerland), *Biogeosciences*, 13, 1587-1596, 10.5194/bg-13-1587-2016, 2016.
- 386 Alewell, C., Pitois, A., Meusburger, K., Ketterer, M., and Mabit, L.: Pu $^{239+240}$ from "contaminant" to
387 soil erosion tracer: Where do we stand?, *Earth-Science Reviews*, 172, 107-123,
388 10.1016/j.earscirev.2017.07.009, 2017.
- 389 Alewell, C., Ringeval, B., Ballabio, C., Robinson, D. A., Panagos, P., and Borrelli, P.: Global
390 phosphorus shortage will be aggravated by soil erosion, *Nature Communications*, 11, 4546,
391 10.1038/s41467-020-18326-7, 2020.
- 392 Amundson, R., Berhe, A. A., Hopmans, J. W., Olson, C., Sztein, A. E., and Sparks, D. L.: Soil and
393 human security in the 21st century, *Science*, 348, 6, 2015.
- 394 Arata, L., Alewell, C., Frenkel, E., A'Campo-Neuen, A., Iurian, A.-R., Ketterer, M. E., Mabit, L., and
395 Meusburger, K.: Modelling Deposition and Erosion rates with RadioNuclides (MODERN) – Part 2: A
396 comparison of different models to convert $^{239+240}\text{Pu}$ inventories into soil redistribution rates at
397 unploughed sites, *Journal of Environmental Radioactivity*, 162–163, 97-106,
398 <http://dx.doi.org/10.1016/j.jenvrad.2016.05.009>, 2016a.
- 399 Arata, L., Meusburger, K., Frenkel, E., A'Campo-Neuen, A., Iurian, A.-R., Ketterer, M. E., Mabit, L.,
400 and Alewell, C.: Modelling Deposition and Erosion rates with RadioNuclides (MODERN) – Part 1: A
401 new conversion model to derive soil redistribution rates from inventories of fallout radionuclides,
402 *Journal of Environmental Radioactivity*, 162–163, 45-55,
403 <http://dx.doi.org/10.1016/j.jenvrad.2016.05.008>, 2016b.
- 404 Avolio, S., Ciancio, O., Grinovero, C., Iovino, F., Mirabella, A., Raglione, M., Sfalanga, M., and Torri,
405 D.: Effetti del tipo di bosco sull'entità dell'erosione in unità idrologiche della Calabria—Modelli
406 erosivi, *Annali Istituto Sperimentale Selvicoltura*, 45–131 pp., 1980.
- 407 Borrelli, P., Robinson, D. A., Fleischer, L. R., Lugato, E., Ballabio, C., Alewell, C., Meusburger, K.,
408 Modugno, S., Schütt, B., Ferro, V., Bagarello, V., van Oost, K., Montanarella, L., and Panagos, P.: An
409 assessment of the global impact of 21st century land use change on soil erosion, *Nature*
410 *Communications*, 8, 2013, 10.1038/s41467-017-02142-7, 2017.
- 411 Cantore, V., Iovino, F., and Puglisi, S.: Influenza della forma di governo sui deflussi liquidi e solidi in
412 piantagioni di eucalitti, *L'Italia Forestale e Montana*, 5, 463-477, 1994.
- 413 Froehlich, M. B., Dietze, M. M. A., Tims, S. G., and Fifield, L. K.: A comparison of fallout U-236 and
414 Pu-239 uptake by Australian vegetation, *Journal of Environmental Radioactivity*, 151, 558-562,
415 10.1016/j.jenvrad.2015.06.021, 2016.
- 416 Hoo, W. T., Fifield, L. K., Tims, S. G., Fujioka, T., and Mueller, N.: Using fallout plutonium as a probe
417 for erosion assessment, *Journal of Environmental Radioactivity*, 102, 937-942,
418 10.1016/j.jenvrad.2010.06.010, 2011.
- 419 IAEA: Guidelines for using Fallout radionuclides to assess erosion and effectiveness of soil
420 conservation strategies, International Atomic Energy Agency, Vienna, Austria, 213, 2014.
- 421 Kato, H., Onda, Y., and Tanaka, Y.: Using Cs-137 and Pb-210(ex) measurements to estimate soil
422 redistribution rates on semi-arid grassland in Mongolia, *Geomorphology*, 114, 508-519,
423 10.1016/j.geomorph.2009.08.009, 2010.
- 424 Kelley, J. M., Bond, L. A., and Beasley, T. M.: Global distribution of Pu isotopes and ^{237}Np , *Science*
425 *of the Total Environment*, 237-238, 483-500, 10.1016/s0048-9697(99)00160-6, 1999.

426 Ketterer, M. E., Hafer, K. M., Link, C. L., Kolwaite, D., Wilson, J., and Mietelski, J. W.: Resolving
427 global versus local/regional Pu sources in the environment using sector ICP-MS, *Journal of Analytical*
428 *Atomic Spectrometry*, 19, 241-245, 10.1039/b302903d, 2004.

429 Ketterer, M. E., Zheng, J., and Yamada, M.: Applications of Transuranics as Tracers and Chronometers
430 in the Environment, *Handbook of Environmental Isotope Geochemistry*, Vols 1 and 2, edited by:
431 Baskaran, M., Springer-Verlag Berlin, Berlin, 395-417 pp., 2011.

432 Lal, R., Tims, S. G., Fifield, L. K., Wasson, R. J., and Howe, D.: Applicability of Pu-239 as a tracer for
433 soil erosion in the wet-dry tropics of northern Australia, *Nucl. Instrum. Methods Phys. Res. Sect. B-*
434 *Beam Interact. Mater. Atoms*, 294, 577-583, 10.1016/j.nimb.2012.07.041, 2013.

435 Lujanienė, G., Plukis, A., Kimtys, E., Remeikis, V., Jankunaite, D., and Ogorodnikov, B. I.: Study of
436 Cs-137, Sr-90, Pu-239, Pu-240, Pu-238 and Am-241 behavior in the Chernobyl soil, *Journal of*
437 *Radioanalytical and Nuclear Chemistry*, 251, 59-68, 10.1023/a:1015185011201, 2002.

438 Mabit, L., Benmansour, M., and Walling, D. E.: Comparative advantages and limitations of the fallout
439 radionuclides Cs-137, Pb-210(ex) and Be-7 for assessing soil erosion and sedimentation, *Journal of*
440 *Environmental Radioactivity*, 99, 1799-1807, 10.1016/j.jenvrad.2008.08.009, 2008.

441 Mabit, L., Benmansour, M., Abril, J. M., Walling, D. E., Meusburger, K., Iurian, A. R., Bernard, C.,
442 Tarján, S., Owens, P. N., Blake, W. H., and Alewell, C.: Fallout $^{210}\text{Pb}_{\text{ex}}$ as a soil and sediment tracer in
443 catchment sediment budget investigations: A review, *Earth-Science Reviews*, 138, 335-351, 2014.

444 Matisoff, G., Bonniwell, E. C., and Whiting, P. J.: Soil erosion and sediment sources in an Ohio
445 watershed using beryllium-7, cesium-137, and lead-210, *Journal of Environmental Quality*, 31, 54-61,
446 2002.

447 Meusburger, K., Mabit, L., Ketterer, M., Park, J.-H., Sandor, T., Porto, P., and Alewell, C.: A multi-
448 radionuclide approach to evaluate the suitability of Pu239+240 as soil erosion tracer, *Science of the*
449 *Total Environment*, 566, 1489-1499, 10.1016/j.scitotenv.2016.06.035, 2016.

450 Meusburger, K., Porto, P., Mabit, L., La Spada, C., Arata, L., and Alewell, C.: Excess Lead-210 and
451 Plutonium-239+240: Two suitable radiogenic soil erosion tracers for mountain grassland sites,
452 *Environmental Research*, 160, 195-202, 10.1016/j.envres.2017.09.020, 2018.

453 Meusburger, K., Evrard, O., Alewell, C., Borrelli, P., Cinelli, G., Ketterer, M., Mabit, L., Panagos, P.,
454 van Oost, K., and Ballabio, C.: Plutonium aided reconstruction of caesium atmospheric fallout in
455 European topsoils, *Sci Rep*, 10, 11858, 10.1038/s41598-020-68736-2, 2020.

456 Michelotti, E. A., Whicker, J. J., Eisele, W. F., Breshears, D. D., and Kirchner, T. B.: Modeling aeolian
457 transport of soil-bound plutonium: considering infrequent but normal environmental disturbances is
458 critical in estimating future dose, *Journal of Environmental Radioactivity*, 120, 73-80,
459 10.1016/j.jenvrad.2013.01.011, 2013.

460 Panagos, P., Imeson, A., Meusburger, K., Borrelli, P., Poesen, J., and Alewell, C.: Soil Conservation in
461 Europe: Wish or Reality?, *Land Degradation & Development*, 27, 1547-1551, 10.1002/ldr.2538, 2016.

462 Porto, P., Walling, D. E., and Ferro, V.: Validating the use of caesium-137 measurements to estimate
463 soil erosion rates in a small drainage basin in Calabria, Southern Italy, *Journal of Hydrology*, 248, 93-
464 108, 10.1016/s0022-1694(01)00389-4, 2001.

465 Porto, P., Walling, D. E., Ferro, V., and Di Stefano, C.: Validating erosion rate estimates provided by
466 caesium-137 measurements for two small forested catchments in Calabria, southern Italy, *Land*
467 *Degradation & Development*, 14, 389-408, 10.1002/ldr.561, 2003.

468 Porto, P., and Walling, D. E.: Validating the use of Cs-137 and Pb-210(ex) measurements to estimate
469 rates of soil loss from cultivated land in southern Italy, *Journal of Environmental Radioactivity*, 106,
470 47-57, 10.1016/j.jenvrad.2011.11.005, 2012.

471 Porto, P., Walling, D. E., and Callegari, G.: Using ^{137}Cs and $^{210}\text{Pb}_{\text{ex}}$ measurements to investigate the
472 sediment budget of a small forested catchment in southern Italy, *Hydrological Processes*, 27, 795-806,
473 10.1002/hyp.9471, 2013.

474 Porto, P., Walling, D. E., Alewell, C., Callegari, G., Mabit, L., Mallimo, N., Meusburger, K., and
475 Zehringer, M.: Use of a ^{137}Cs re-sampling technique to investigate temporal changes in soil erosion
476 and sediment mobilization for a small forested catchment in southern Italy, *Journal of Environmental*
477 *Radioactivity*, 138, 137-148, 2014.

478 Porto, P., Cogliandro, V., and Callegari, G.: Exploring the performance of the SEDD model to predict
479 sediment yield in eucalyptus plantations. Long-term results from an experimental catchment in
480 Southern Italy, *IOP Conference Series: Earth and Environmental Science*, 107, 012020, 10.1088/1755-
481 1315/107/1/012020, 2018.

482 Porto, P., Bacchi, M., Preiti, G., Romeo, M., and Monti, M.: Combining plot measurements and a
483 calibrated RUSLE model to investigate recent changes in soil erosion in upland areas in Southern Italy,
484 *J. Soils Sediments*, 22, 1010-1022, 10.1007/s11368-021-03119-2, 2022.

485 Porto, P., and Callegari, G.: Comparing long-term observations of sediment yield with estimates of soil
486 erosion rate based on recent Cs-137 measurements. Results from an experimental catchment in Southern
487 Italy, *Hydrological Processes*, 36, 10.1002/hyp.14663, 2022.

488 Qiao, J. X., Hansen, V., Hou, X. L., Aldahan, A., and Possnert, G.: Speciation analysis of I-129, Cs-
489 137, Th-232, U-238, Pu-239 and Pu-240 in environmental soil and sediment, *Applied Radiation and*
490 *Isotopes*, 70, 1698-1708, 10.1016/j.apradiso.2012.04.006, 2012.

491 Reichstein, M., Bahn, M., Ciais, P., Frank, D., Mahecha, M. D., Seneviratne, S. I., Zscheischler, J.,
492 Beer, C., Buchmann, N., Frank, D. C., Papale, D., Rammig, A., Smith, P., Thonicke, K., van der Velde,
493 M., Vicca, S., Walz, A., and Wattenbach, M.: Climate extremes and the carbon cycle, *Nature*, 500, 287-
494 295, 10.1038/nature12350, 2013.

495 Schimmack, W., Auerswald, K., and Bunzl, K.: Can Pu239+240 replace Cs-137 as an erosion tracer in
496 agricultural landscapes contaminated with Chernobyl fallout?, *Journal of Environmental Radioactivity*,
497 53, 41-57, 10.1016/s0265-931x(00)00117-x, 2001.

498 Sorriso-Valvo, M., Bryan, R. B., Yair, A., Iovino, F., and Antronico, L.: Impact of afforestation on
499 hydrological response and sediment production in a small Calabrian catchment, *CATENA*, 25, 89-104,
500 [https://doi.org/10.1016/0341-8162\(95\)00002-A](https://doi.org/10.1016/0341-8162(95)00002-A), 1995.

501 Teramage, M. T., Onda, Y., Wakiyama, Y., Kato, H., Kanda, T., and Tamura, K.: Atmospheric Pb-210
502 as a tracer for soil organic carbon transport in a coniferous forest, *Environ. Sci.-Process Impacts*, 17,
503 110-119, 10.1039/c4em00402g, 2015.

504 Tims, S. G., Everett, S. E., Fifield, L. K., Hancock, G. J., and Bartley, R.: Plutonium as a tracer of soil
505 and sediment movement in the Herbert River, Australia, *Nucl. Instrum. Methods Phys. Res. Sect. B-*
506 *Beam Interact. Mater. Atoms*, 268, 1150-1154, 10.1016/j.nimb.2009.10.121, 2010.

507 Wallbrink, P. J., and Murray, A. S.: Determining soil loss using the inventory ratio of excess lead-210
508 to cesium-137, *Soil Science Society of America Journal*, 60, 1201-1208, 1996.

509 Walling, D. E., He, Q., and Appleby, P. G.: Conversion models for use in soil-erosion, soil-
510 redistribution and sedimentation investigations, in: *Handbook for the Assessment of Soil Erosion and*
511 *Sedimentation using Environmental Radionuclides*, edited by: Zapata, F., The Netherlands, 111-164,
512 2002.

513 Walling, D. E., Zhang, Y., and He, Q.: Conversion models and related software, in: *Guidelines for*
514 *Using Fallout Radionuclides to Assess Erosion and Effectiveness of Soil Conservation Strategies*,
515 *IAEA-TECDOC-1741*, Vienna, 125-148, 2014.

516 Wilken, F., Fiener, P., Ketterer, M., Meusburger, K., Muhindo, D. I., van Oost, K., and Doetterl, S.:
517 Assessing soil redistribution of forest and cropland sites in wet tropical Africa using $^{239+240}\text{Pu}$ fallout
518 radionuclides, *SOIL*, 7, 399-414, 10.5194/soil-7-399-2021, 2021.

519 Wood, S. N.: Low-rank scale-invariant tensor product smooths for generalized additive mixed models,
520 *Biometrics*, 62, 1025-1036, 10.1111/j.1541-0420.2006.00574.x, 2006.

521 Xiao, H., Liu, G., Liu, P., Zheng, F., Zhang, J., and Hu, F.: Sediment transport capacity of concentrated
522 flows on steep loessial slope with erodible beds, *Sci Rep*, 7, 2350, 10.1038/s41598-017-02565-8, 2017.

523 Xu, Y., Pan, S., Wu, M., Zhang, K., and Hao, Y.: Association of Plutonium isotopes with natural soil
524 particles of different size and comparison with ¹³⁷Cs, *Science of The Total Environment*, 581-582,
525 541-549, <https://doi.org/10.1016/j.scitotenv.2016.12.162>, 2017.

526 Xu, Y. H., Qiao, J. X., Hou, X. L., and Pan, S. M.: Plutonium in Soils from Northeast China and Its
527 Potential Application for Evaluation of Soil Erosion, *Sci Rep*, 3, 10.1038/srep03506, 2013.

528 Xu, Y. H., Qiao, J. X., Pan, S. M., Hou, X. L., Roos, P., and Cao, L. G.: Plutonium as a tracer for soil
529 erosion assessment in northeast China, *Science of the Total Environment*, 511, 176-185,
530 10.1016/j.scitotenv.2014.12.006, 2015.

531 Zapata, F.: The use of environmental radionuclides as tracers in soil erosion and sedimentation
532 investigations: recent advances and future developments, *Soil & Tillage Research*, 69, 3-13, 2003.

533 Zhou, G. Y., Morris, J. D., Yan, J. H., Yu, Z. Y., and Peng, S. L.: Hydrological impacts of reafforestation
534 with eucalypts and indigenous species: a case study in southern China, *Forest Ecology and
535 Management*, 167, 209-222, [https://doi.org/10.1016/S0378-1127\(01\)00694-6](https://doi.org/10.1016/S0378-1127(01)00694-6), 2002.

536 Zuazo, V. c. H. D., and Pleguezuelo, C. R. o. R.: Soil-Erosion and Runoff Prevention by Plant Covers:
537 A Review, in: *Sustainable Agriculture*, edited by: Lichtfouse, E., Navarrete, M., Debaeke, P.,
538 Véronique, S., and Alberola, C., Springer Netherlands, Dordrecht, 785-811, 2009.

539